Commentary on API 653 Annex B "Evaluation of Tank Bottom Settlement"

January 20, 2023

Summary

API 653 Annex B *Evaluation of Tank Bottom Settlement* permits two methods of evaluating settlement. The original method is due to Marr, et al. [1], and the newer method due to Andreani, et al. [2]. This paper revisits API 653 B, in response to reported problems with Marr's method and in the light of the much more detailed and accurate data provided by 3D laser scanning.

Both methods (Marr and Andreani) were originally developed for analyzing a small number of elevations taken at measurement stations, typically evenly spaced 16 to 32 feet apart around the bottom circumference.

Both methods aim to set upper bounds on maximum curvature of vertical deflections along the bottom edge of the tank shell, which indirectly puts a bound on ovalization at the top of the tank[1]. At a locally maximum deflection, curvature equals the negative second derivative of the out-of-plane deflection curve $u(\ell)$ with respect to arc length ℓ. Marr's method is based on Malik, et al. [3] who used a second divided difference approximation to the second derivative (their equation (2)).

As we'll show, the second divided difference computed from widely spaced points can substantially underestimate true curvature, which accounts for the poor performance of Marr's method [4] for widely spaced measurement stations.

---

[1] See Malic, Morton, and Ruiz [3], Appendix 1, "An Estimate of the Radial Displacement of the Top of a Cylindrical Tank."

Andreani's method sets an upper bound on the maximum deflection in an arc bounded by zeroes (see Figure 5). It was calibrated against finite element analyses of single folds ranging from 20 feet, measured across the bottom of the tank, up to the full diameter. We re-express their upper bound as a bound on an asymmetric divided difference, see Equation (29). This allowed us to directly compare Marr's and Andreani's upper bounds and we can report that Marr's bound permits much higher curvature compared to Andreani's better calibrated bound (Table 2). This raises a problem because API 653 B makes Marr's method the gatekeeper for using Andreani's method,

> *"**B.2.2.5.2** If … the maximum out-of-plane settlement determined in accordance with B.3.2.1 [Marr's method] is exceeded, the procedure in B.3.2.2 [Andreani's method] may be used to evaluate the settlement"*

Thus API 653 B does not permit Andreani's method to correct *false negatives*, occasions when Marr's method fails to detect excess strain.

Marr's divided difference estimate of the second derivative is increasingly dominated by noise as spacing between measurement stations gets smaller. To ameliorate this API 653 B suggests skipping points to increase the spacing,

> *"[when] the arc length L between measurement points is small. It is acceptable to … only use a subset of these points spaced no further than 32 ft [apart]"*

We have found that the spacing should be 16 to 20 ft to balance bias and noise. If the spacing is shorter, the divided second difference is mostly noise, and if it is longer the divided difference is less noisy but substantially underestimates the second derivative, Figure 11.

3D laser scanning produces a dense point-cloud of bottom edge elevations a few inches apart, Figure 12. This abundance of closely-spaced data permits the analyst to reduce the noise and bias problems associated with Marr's method. Our proposed *Trigonometric-Fit* methodology[2] fits a band-pass Fourier cosine series to the elevation data to remove rigid tilt and high frequency noise, and calculates the second derivative of the Fourier series.

The suggestion of differentiating a Fourier series fitted to the data goes as far back as 1977 [3] but the sparse, manually measured elevation measurements of that era were judged too noisy for the purpose. However, dense, accurate laser-scan data is ideal for Fourier analysis.

---

[2] Fitting a Fourier series to elevation measures was suggested in [6]. We use the series to filter out noise and estimate true second derivative at each perimeter point when closely spaced data are available.

Review of API 653 Annex B

The shell of an atmospheric petroleum storage tank will experience additional bending stress at any point where the curvature has changed from its original equilibrium value. API 653 B is concerned with bending stresses induced by tank settlement. This paper addresses edge settlement but not local interior settling.

Rigid Settlement with Planar tilt

In this mode, the tank settles vertically while rotating around a line in the horizontal plane (the *strike azimuth*[3]) (see Figure 2 panel B). Elevation at the bottom of the settled shell follows a cosine curve as a function of arc length along the shell bottom measured in feet clockwise from north. However, rigid tilt does not change the curvature at any point on the tank shell and therefore does not introduce bending stress.
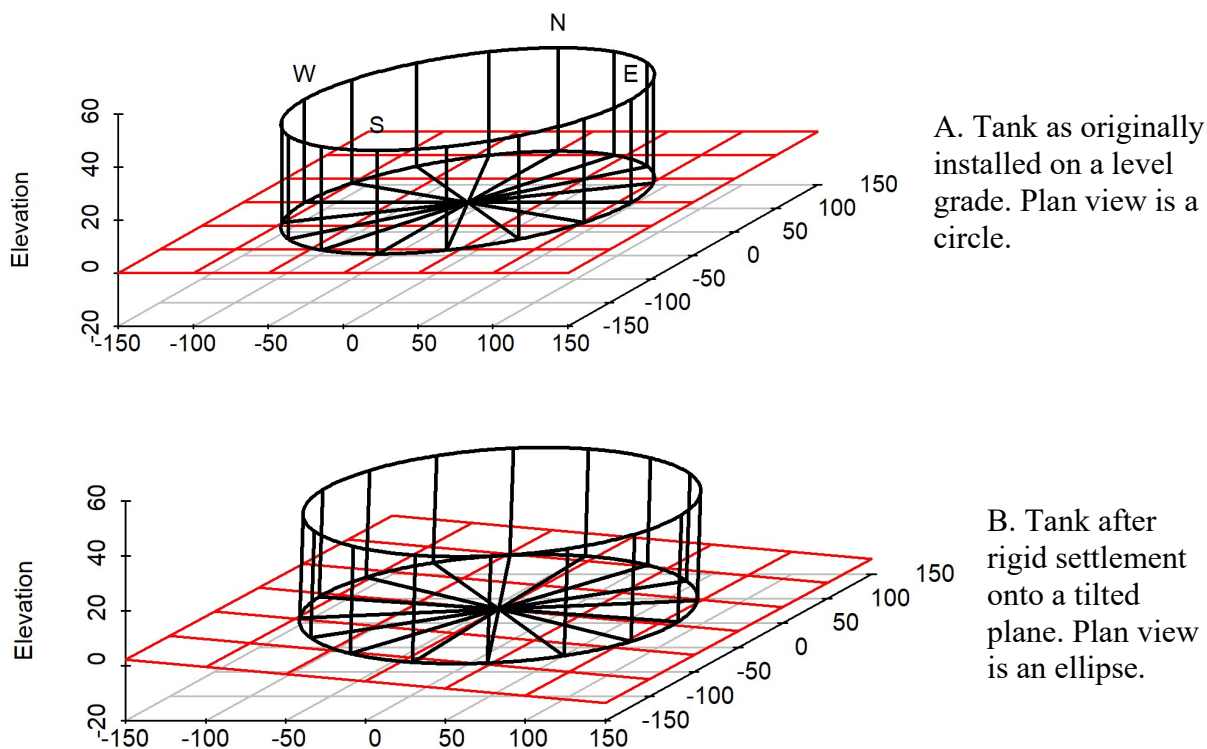
A. Tank as originally installed on a level grade. Plan view is a circle.

B. Tank after rigid settlement onto a tilted plane. Plan view is an ellipse.

Figure 1. Tank Settlement with Rigid Tilt.

---

[3] Azimuth is the angle (measured clockwise from north) of a line from the center of the tank to a point on its circumference. The dip azimuth points toward the lowest point on the circumference. Settlement is typically negative but amplitude can be positive or negative.
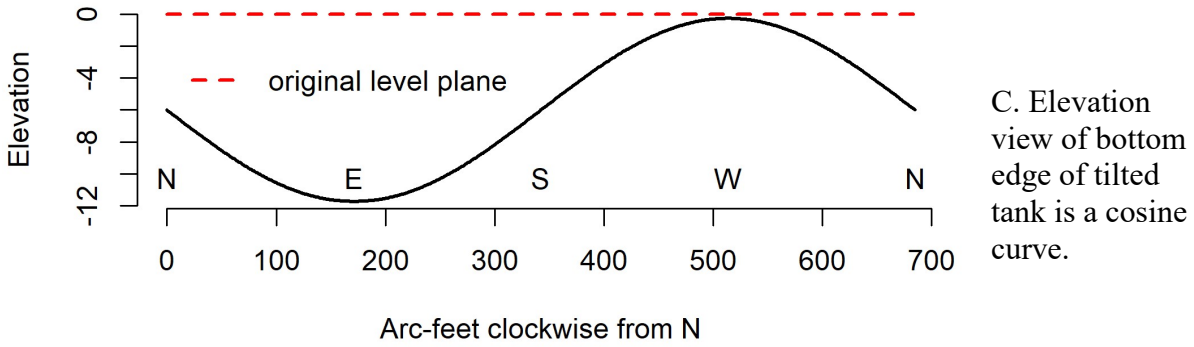
C. Elevation view of bottom edge of tilted tank is a cosine curve.

Figure 2. Elevation of Bottom Edge after Settlement with Rigid Tilt

Computing the Rigid Tilt Plane via Multiple Linear Regression

Elevation (relative to the original level grade) of the tilted tank bottom at azimuth θ is,

$$Z(\theta) = A \cdot \cos(\theta - \varphi) + \Delta s \text{ , where} \tag{1}$$

A : signed amplitude, Δs : signed average settlement

θ : azimuth of a point on the bottom edge (clockwise from north),

φ : phase angle, and $\varphi + \pi \cdot (A > 0)$ = dip azimuth (steepest downhill direction)

$\delta = |A/Radius|$ is the slope along the dip azimuth.

In Figure 4 we show how to use the regression tool[4] in MS Excel© to estimate the tilt plane. The data are elevation measures (Z) taken at 16 evenly spaced stations around the base of the shell relative to an arbitrary reference elevation (benchmark, or datum). The diameter of the tank is 120 feet, so the circumference is π×120 = 377 feet. The spacing between stations is 377/16 = 23.56 feet. Column "theta" is the number of radians clockwise from station 1; theta = 2×π×(Station-1)/16. "cos" and "sin" are the cosines and sines of theta. We instructed Excel to regress settlement on cosine and sine. The result is,

$$\hat{z}(\theta) = -1.147 - 0.332 \cdot \cos(\theta) - 0.408 \cdot \sin(\theta)$$

The spreadsheet converts this to a cosine with phase angle by using the trigonometric identity,

$$a \cdot \cos(\theta) + b \cdot \sin(\theta) = A \cdot \cos(\theta - \varphi),$$

---

[4] PEMY Consulting provides an example calculation on github at the URL

https://github.com/rbitip/settlement-excel-regression-too

where the signed amplitude is $A = \operatorname{sgn}(a) \cdot \sqrt{a^2 + b^2} = -0.526$, and the phase angle is $\varphi = \arctan(b/a) = 0.889$.

Elevation along the bottom edge on the tilt-plane, Equation (1), is,

$$\hat{z}(\theta) = -1.147 - 0.526 \cdot \cos(\theta - 0.889) = -\Delta s + A \cdot \cos(\theta - \varphi), \text{ where} \qquad (2)$$

Δs is *average settlement*, A is *amplitude*, and $\varphi = 0.889$ radians is the *phase angle* measured counter-clockwise from the first measurement station[5]. Regression residuals $U = Z - \hat{z}$ are called "out-of-plane (OOP) deflections".

Figure 3 (left panel) is a graph of raw elevations (Z) and the cosine model that best fits the data. Out-of-plane deflection at the 9th measurement station is the blue arrow in each panel. Out-of-plane deflection, shown in the right panel, does induce bending strain, which we will examine next.
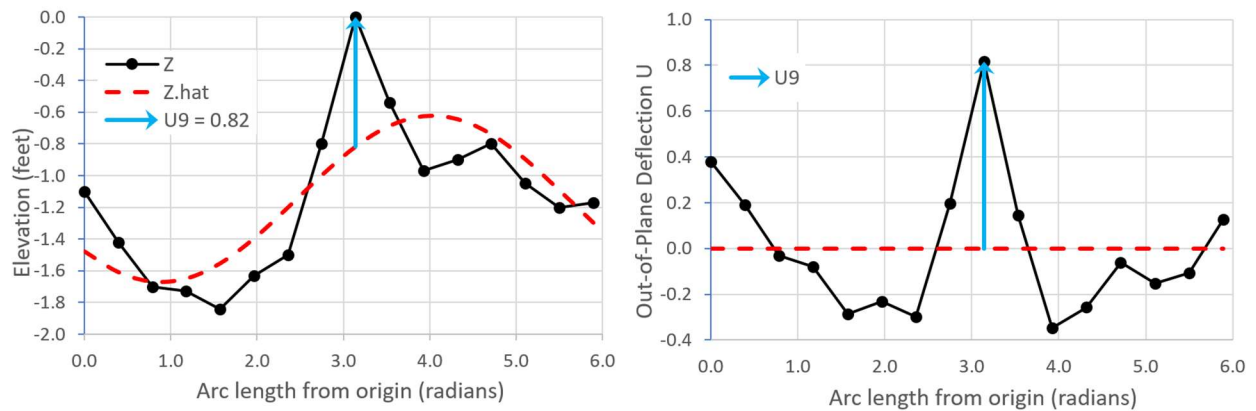

Figure 3. Left: Excel plot of Settlement and Tilt-Plane. Right: Out-of-plane Deflection (ft).

---

[5] For these data, we do not know the x-y coordinates of the measurement stations. Therefore, the azimuth of the first measurement station is arbitrarily set to zero.

Tank Data		Computed Values (do not enter)					Regression on cos and sin.					
Station	Z^a	theta	cos	sin	$Z.fit^b$	U^c	Regression Stats		Computed Parameters			
1	-1.10	0.000	1.00	0.00	-1.48	0.38	Adj R Sqr	0.558	Amplitude		-0.526	inch
2	-1.42	0.393	0.92	0.38	-1.61	0.19	Resid se	0.325	Phase		0.888	rad
3	-1.70	0.785	0.71	0.71	-1.67	-0.03	n	16				
4	-1.73	1.178	0.38	0.92	-1.65	-0.08	Analysis of Variance Table					
5	-1.84	1.571	0.00	1.00	-1.56	-0.28	Source	df	SS	MS	F	p-val
6	-1.63	1.963	-0.38	0.92	-1.40	-0.23	Tilt	2	2.214	1.107	10.46	0.002
7	-1.50	2.356	-0.71	0.71	-1.20	-0.30	Residual	13	1.376	0.106		
8	-0.80	2.749	-0.92	0.38	-1.00	0.20	Regression Coefficients					
9	0.00	3.142	-1.00	0.00	-0.82	0.82		Est	se	p-val	95% Conf. Int.	
10	-0.54	3.534	-0.92	-0.38	-0.68	0.14	Intercept	-1.147	0.081	0.000	-1.32	-0.97
11	-0.97	3.927	-0.71	-0.71	-0.62	-0.35	cos(theta)	-0.332	0.115	0.006	-0.58	-0.08
12	-0.90	4.320	-0.38	-0.92	-0.64	-0.26	sin(theta)	-0.408	0.115	0.002	-0.66	-0.16
13	-0.80	4.712	0.00	-1.00	-0.74	-0.06	Definitions					
14	-1.05	5.105	0.38	-0.92	-0.90	-0.15	a) Z: elevation of tank bottom relative to original grade					
15	-1.20	5.498	0.71	-0.71	-1.09	-0.11	b) Z.fit: best-fit tilt plane					
16	-1.17	5.890	0.92	-0.38	-1.30	0.13	c) U = (Z − Z.fit): out-of-plane deflection					

Figure 4. Planar tilt for Andreani's[6] example 2. The complement of the *p*-value, 1-p = 0.998, is the analyst's *confidence*[7] in saying "the tilt angle is not zero."

"Validity" of the tilt-plane: role of adjusted R^2 and *p* value:

Adjusted R^2 is a measure of how much of the total variance of the raw elevations is accounted for by the tilt-plane. The tilt-plane analysis in Figure 3 had adj R^2 = 0.558, meaning that the sinusoidal variation of the tilt plane around the bottom of the tank accounted for 55.8% of the variance of the raw elevations. The remaining 44.2% is due to noise and higher-order out-of-plane warping. Contrary to API 653 B[8], adjusted R^2 is *not* a test of whether the tilt-plane is "valid"; that is the job of the *p*-value. For the case of the tilt-plane analysis in Figure 3, the *p*-value was 0.002,

---

[6] The data in Figure 4 (Andreani et al.'s Example 2 in [2]) are 16 equally-spaced settlement measurements around the perimeter of a 120 x 40 foot (Diameter x Height) floating roof tank.

[7] Confidence and its Bayesian analogue, *credibility*, are complicated topics. Saying "I am 99.8% confident that the bottom is tilted," means, "if there were no real tilt, then there is only 0.2% probability that the estimated tilt will be this big."

[8] API 653 Paragraph B.2.2.4 e) wrongly states, "[a] cosine curve is only considered valid … if the value of R^2 is greater than or equal to 0.9."

which indicates that the tilt plane is highly *statistically significant* (highly unlikely to be a noise artifact). Conventionally *p*-values below 0.05 are considered statistically significant[9].

API Differential Settlement Analysis

The current authoritative resource for large assessing flat bottom tank differential settlement is API 653 Annex B "Evaluation of Tank Bottom Settlement". Differential settlement may be local or global bulges and dishing, or settlement near the shell that deviates from the cosine curve. Many researchers have contributed to the settlement criteria used today. While local and global bulges and dishing can be analyzed by simplified models such as those given in stress analysis textbooks, differential settlement has defied even approximate solutions until recently. API 653 Annex B offers two of those approximate methods. However, these should be viewed as screening methods that identify possible areas of excess stress needing follow-up. Ultimately, finite element analysis should be considered the gold standard.

Overview of API 653 Annex B Methods

API 653 5th Edition, Annex B, describes two methods for analyzing out-of-plane settlements and determining whether they are within allowable bounds.

The two methods follow the same general procedure:

1. For given settlement data, calculate the regular 1-mode cosine curve fit.
2. Calculate out-of-plane deflections, U, measured in in the same units as tank circumference (either feet or meters), by subtracting the cosine curve fit from the settlement data ($U_i = Z_i - \hat{z}_i$, where Z is the observed settlement data (feet), $\hat{z}$ is the cosine curve fit, and the subscript *i* denotes that these are their values for measurement station *i*).
3. Three-point out-of-plane settlement values, S_i, are computed at each station and are compared to a maximum permitted value, $S_{\max}$

The first of these, Marr's method [1] is described in API 653 B.2.2.4. In this method, the out-of-plane deflection (U_i for data point *i*) is used to calculate the out-of-plane settlement (S_i). As described in API 653 figure B.3, the out-of-plane settlement at point *i* is

$$S_i = U_i - \left(\frac{1}{2}U_{i-1} + \frac{1}{2}U_{i+1} \right), \tag{3}$$

---

[9] But note that a *control variable*, that corrects *causal variables* for bias, is customarily kept in the model if its *p*-value is less than 0.15. Planar tilt is an example of a control variable: it does not cause stress but it can bias the estimates of warping modes that do cause stress.

The maximum permissible out-of-plane settlement (in feet) for Marr's method, per API 653 B.3.2.1, is[10]

$$S_{max,ft} = \frac{11 \cdot (L^2 \cdot Y)}{2 \cdot (E \cdot H)}$$

(4)

Where,

L is arc length between (evenly spaced) measurement stations, in feet,

Y (or σ_y) is the yield strength of the shell material, assumed to be

E is Young's Modulus of the shell material, and

H is the tank height, in feet.

The second of these two, Andreani's method [2], computes out-of-plane settlement differently. A *settlement arc* is defined as the interval between two successive interpolated zeroes of the graph of out-of-plane deflections, U. Out-of-plane settlement S_i is the maximum vertical deflection (***in inches***) between the ith pair of zeroes, as in Figure 5.
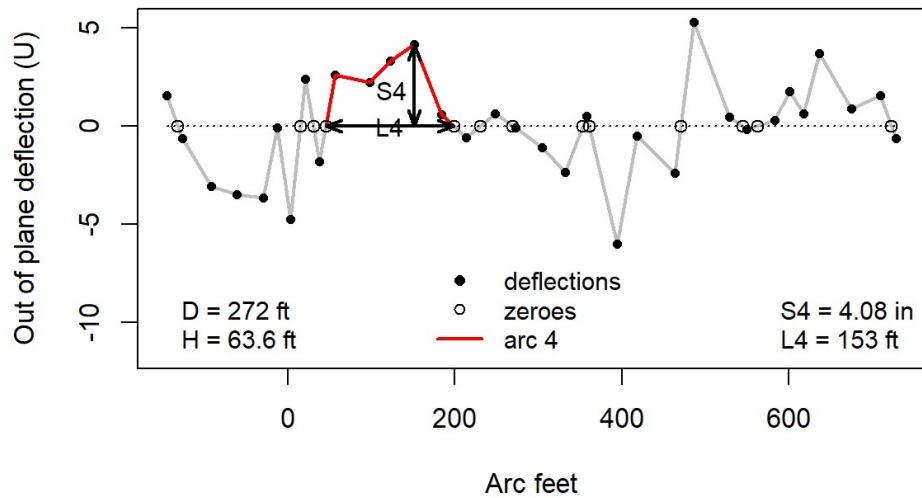

Figure 5. Andreani's Measure of Out-of-plane Settlement (inches).

Maximum permitted out-of-plane settlement (in inches) is,

$$S_{max,in} = \min\left(K \cdot S_{arc,ft} \frac{D}{H} \frac{Y}{E}, 4.0\,in \right)$$

(5)

---

[10] This is one-half the "permissible OOP settlement" proposed in Marr, et al. [4]; presumably, dividing by 2 was intended as as an ad-hoc safety factor.

Where,

K is a tabulated value from Table 1,

$S_{arc,ft}$ = settlement arc length in feet (for example, L4 in Figure 5)

D = tank diameter, ft

H = tank height, ft

Y = yield strength, psi

E = Young's Modulus, psi

Tank Diameter ft	K, Open Top Tanks	K, Fixed Roof Tanks
$D \leq 50$	28.7	10.5
$50 < D \leq 80$	7.8	5.8
$80 < D \leq 120$	6.5	3.9
$120 < D \leq 180$	4.0	2.3
$180 < D \leq 240$	3.6	Not applicable
$240 < D \leq 300$	2.4	Not applicable
$300 < D$	Not applicable	Not applicable

Table 1. API 653 K table from API 653, Section B.3.2.2

Digression: The tilt plane should *always* be subtracted from raw settlement values

In saying this, we directly contradict the advice in API 653 [5], paragraph B.2.2.4:

> *In many cases, the out-of-plane settlement may be concentrated in one or more areas. In such cases, the least-squares fit approach may under predict the local out-of-plane settlement and is not conservative. In these cases, R^2 will typically be less than 0.9, and more rigorous curve-fitting procedures should be considered. Alternatively, the settlement may not indicate a well-defined rigid tilt plane and the procedure in B.2.2.5 should be considered…*

This suggestion is *wrong* and should be ignored; it comes from a misunderstanding of the statistic R^2, a number in the interval [0,1] described as "the proportion of variance explained by the (planar tilt) model". The misunderstanding is the claim that a model is not valid unless R^2 is very high, say 0.9 or above. This is simply not true for several reasons. First, the preferred criterion is *adjusted* R^2. Second, the data may be inherently noisy so that no valid model could have extremely high R^2. Third, candidate exploratory variables are selected solely for their ability to *increase* adjusted R^2. Large R^2 is not required and may be impossible due to measurement noise.

Second Derivative Interpretation of Marr and Andreani Criteria

API felt in the 1990s that there was sufficient research to put limiting rules into API 653 to cover differential settlement. The first rule is based on a paper by Marr et al. [1]. Marr and his co-authors summarized previous work going back to at least the 1960s and concluded that the work of Malik et al. [3] best addressed differential settlement.

Malik, et al. [3], showed[11] that, in theory, ovalizing radial displacement w at the top of a tank shell is directly proportional to the second derivative of out-of-plane deflection function u at the bottom of the shell,

$$w(\ell) = -\frac{D \cdot H}{2} \cdot \frac{d^2 u(\ell)}{d\ell^2} \tag{6}$$

where ℓ is the "hoop coordinate"; i.e., the arc-length (azimuth times radius) measured in feet clockwise from north.

Therefore, it is no surprise that both Marr's and Andreani's criteria can be expressed in terms of upper bounds on approximations of the second derivative of the out-of-plane deflection curve.

Comparison of Marr and Andreani in Terms of Bounding the Second Derivative

Observed out-of-plane deflection U_i, measured in feet at hoop coordinate ℓ_i, is true deflection plus noise,

$$U_i = u(\ell_i) + e_i \tag{7}$$

Bending strain and ovalization are proportional to true curvature κ, which is the inverse radius of the tangent circle at point ℓ,

$$\kappa(\ell) = \frac{u''(\ell)}{\left(1 + u'(\ell)^2\right)^{3/2}} \cong u''(\ell) \tag{8}$$

Menger curvature, $\hat{\kappa}$, is an approximation of true curvature. It is the inverse of the radius of the circle passing through three measured deflections (Figure 6),

$$\hat{\kappa} = \frac{2 \cdot \left(L_{12} \cdot (U_3 - U_2) - L_{23} \cdot (U_2 - U_1) \right)}{d_{12} \cdot d_{23} \cdot d_{13}} \tag{9}$$

---

[11] They give credit to L. M. Langeveld for the original, unpublished derivation.
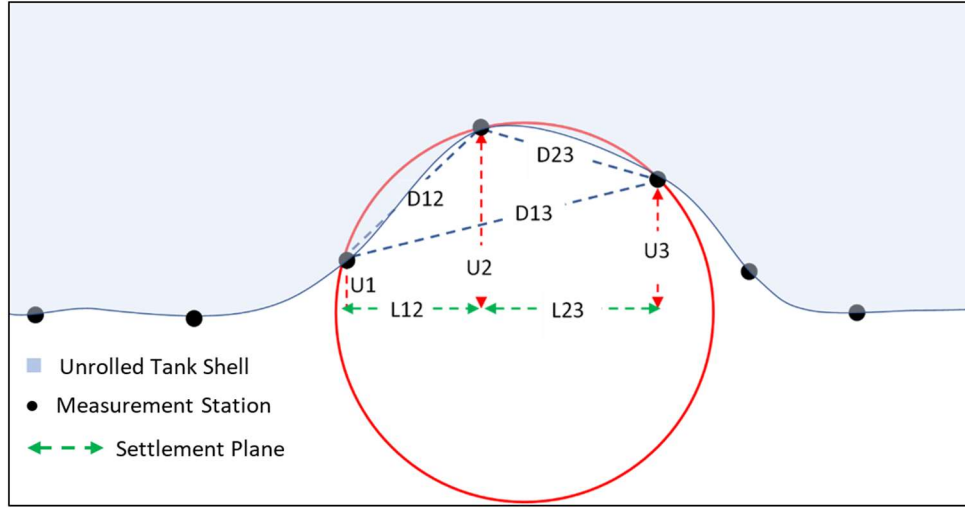
Figure 6. Data for 3-Point Curvature Estimate of a Deflected Section of Tank Shell

In Marr's method, measurement stations are equally spaced so $L_{12} = L_{23} = L$ and Equation (9) becomes[12],

$$\hat{\kappa} = L \cdot 2 \cdot \frac{(U_1 + U_3) - 2 \cdot U_2}{d_{12} \cdot d_{23} \cdot d_{13}} \tag{10}$$

Distance d_{ij} is the hypotenuse of a right triangle with base L_{ij} and height $U_j - U_i$. The difference between the base and the hypotenuse is negligible because distance between stations is on the order of 20 feet and out-of-plane deflections are in the range ±4"; consequently,

$$
\begin{aligned}
\hat{\kappa} \quad &\cong \quad L \cdot 2 \cdot \frac{(U_1 + U_3) - 2 \cdot U_2}{L_{12} \cdot L_{23} \cdot L_{13}} \\
&= \quad L \cdot 2 \cdot \frac{(U_1 + U_3) - 2 \cdot U_2}{L^2 \cdot (2 \cdot L)} \quad , \\
&= \quad 2 \cdot \frac{(U_1 + U_3)/2 - U_2}{L^2} = -\frac{2 \cdot S_2}{L^2}
\end{aligned}
\tag{11}
$$

where S_2 is out-of-plane settlement, Equation (3), at measurement station 2. The expression $2 \cdot S_i / L^2$ is a *second divided difference* that approximates the second derivative.

---

[12] Factor 2L in the denominator comes from $L_{13} = L_{12} + L_{23} = 2 \cdot L$.

Marr's Bound on The Second derivative

Marr, et al. in effect, approximated the second derivative at each measurement station using three adjacent out-of-plane deflection measurements, U_1, U_2, U_3 as shown in Figure 6.

From Equations (8) and (11) we get,

$$S_i = U_i - \frac{U_{i-1} + U_{i+1}}{2} \cong \frac{u''(\ell_i) \cdot L^2}{2}, \tag{12}$$

where L is the (uniform) distance (feet) between measurement stations, and out-of-plane deflections, U, are measured in feet.

Marr's original criterion[13] for a safe amount of out-of-plane deflection was,

$$|S_i| \leq 11 \cdot \frac{L^2 \cdot \sigma_f}{H \cdot E}, \tag{13}$$

where,

L is arc length between (evenly spaced) measurement points, in feet,
σ_y is the yield strength of the shell material, 36 ksi for A36 steel,
E is Young's Modulus of the shell material, 29,000 ksi for A36 steel, and
H is tank height, in feet (ft).

However API 653, without explanation but possibly as a safety factor of 2, used the criterion,

$$|S_i| \leq \frac{11 \cdot L^2 \cdot \sigma_f}{2 \cdot H \cdot E} = S_{\max, ft} \tag{14}$$

Which, via Equation (12), gives what we'll call Marr's bound on the second derivative[14],

$$|u''(\ell_i)| \leq 11 \cdot \frac{\sigma_y}{H \cdot E} = D2_{\max, ft}, \tag{15}$$

---

[13] Equation 11 in reference [1].

[14] The left side unit is ft^{-1} and, on the right, the constant 11 is unitless as is yield strength over Young's modulus so the net unit is also ft^{-1}.

When deflections are measured in inches, the second derivative has units inches/foot², and Marr's bound becomes,

$$\left| u''\left(\ell_i \right) \right| \le 12 \cdot 11 \cdot \frac{\sigma_y}{H \cdot E} = D2_{max,in} \tag{16}$$

Adapting Marr's Criterion to Laser-Scan Data

When stations are closer than 8 feet, API 653 B.2.2.4 says,

> … It is acceptable to [use] all measurement points to develop the optimum cosine curve, but only use a subset of these points spaced no further than 32 ft (8 minimum) when calculating S_i and S_{max}. The points used must include the points furthest from the optimum cosine curve. For example, if 8 points are required, but 16 measurements are taken, and the arc length between measurement points is only 15 ft, calculate the optimum cosine curve using all 16 points, but use only 8 points to calculate S_i

Figure 7 shows 3355 elevation measurements around the bottom edge of a 272 by 66 ft tank (D x H). Following API 653's suggestion, let's "thin" the data to L=20 feet between measurement points. The circumference is 854.5 ft, so there are about 78 points per 20 feet.
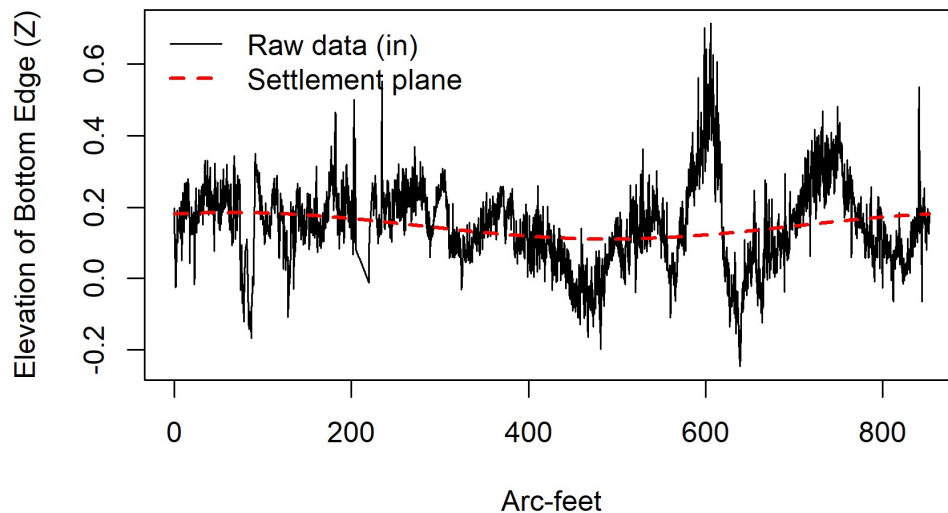

Figure 7. Bottom Edge Elevations in feet of a 272 x 66 ft Tank (D x H).

Assuming equal spacing[15], we'd use every 78th point to compute S's, amounting to 43 S's in all. API says to start at the largest deviation (U) and retain every 78th point. For example, if U_1 happened to be the largest, we'd use points 1, 79, 157, … 3277, and 3355. We did this 9 more times with the starting point shifted by L/10 (in this case shifted by a count of 8). So, the first shift uses points 9, 89, … ,3285, 3363, etc.

Figure 8 shows what that looks like. As a bonus we get an impression of the influence of noise and a "vote" on whether the deflection at 600 feet really exceeds the settlement limit S_{max}. Only two out of 10 shifts exceeds $S_{max,ft}$ so, informally, there's a 20% chance that there is excess out-of-plane settlement.

A weakness of Marr's method is that it is highly sensitive to L, the distance between stations, as illustrated in Figure 9. The settlement limit (the red dotted line) gets larger as the distance (L) between stations increases. Later we'll show that this is caused by bias: the second divided difference underestimates the second derivative and the underestimate becomes worse as distance L between points gets bigger (see Figure 11).
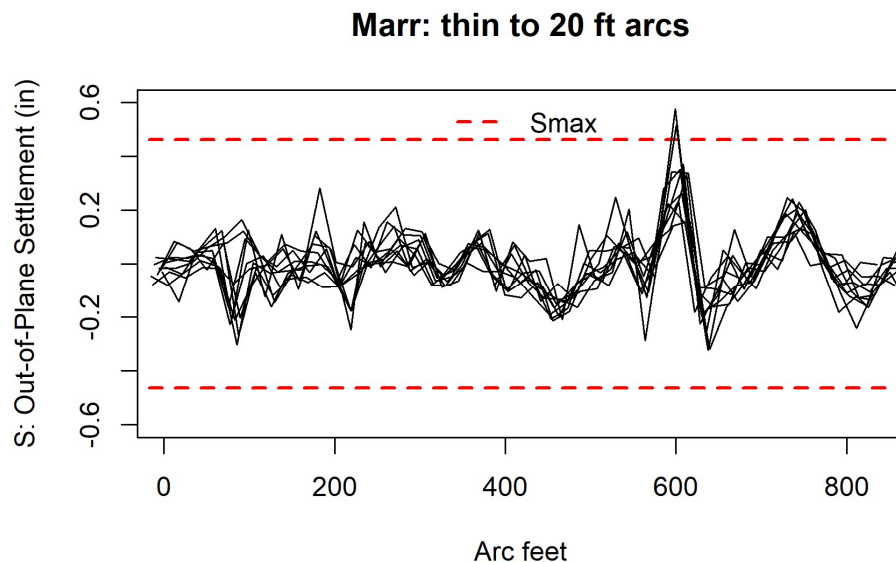
Marr: thin to 20 ft arcs

Figure 8. Marr's method with L=20 for laser-scan data.

---

[15] When spacing is unequal or has gaps points should be selected by distance rather than count.
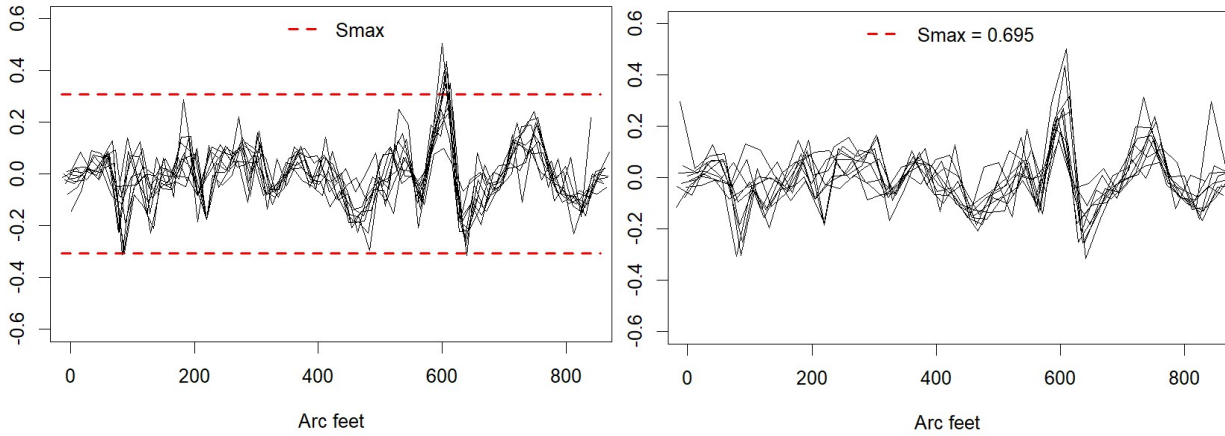
Figure 9. Marr's method with L = 16 feet (left) and 24 feet (right). Note that Smax is off the chart when L=24 feet.

Why Marr's Method fails for wide spacing, L.

Marr's method assumes that the divided second difference of the deflection function is a good approximation of its second derivative. The deflection function u is periodic and therefore can be represented as a Fourier series,

$$u(\ell) = \sum_{k=2}^{k_{max}} A_k \cdot \cos\left(k \cdot \frac{\ell}{R} - \varphi_k\right) \tag{17}$$

The second derivative can be computed term by term,

$$u''(\ell) = -\sum_{k=2}^{k_{max}} (k/R)^2 \cdot A_k \cdot \cos\left(k \cdot \frac{\ell}{R} - \varphi_k\right) \tag{18}$$

where ℓ is the arc length (ft) clockwise from north, R is the radius, ℓ/R is the arc length in radians, k is the period of each term, (cycles per circumference). Parameter A_k is the amplitude of that period, and φ_k is the phase angle. The maximum permitted period, k_{max} is selected so that the shortest half-wave is 20 feet[16]. For the 272 ft diameter tank in Figure 7, that is,

$$k_{max} = \pi \cdot D_{ft} / \left(2 \cdot 20_{ft}\right) = \pi \cdot 272/40 \simeq 21 \tag{19}$$

---

[16] The "sweet spot", balancing noise and bias for Marr's method, is about 20 feet, and Andreani's method was calibrated for 20 foot or longer folds; i.e., settlement arcs longer than 2*R*asin(10/R), where R is the radius of the tank.

There is no constant or first-order term in equation (17) because they were removed by subtracting the tilt plane.

Figure 10 shows the observed out-of-plane deflections in inches (gray), and the finite Fourier series (black), fitted to the data underlying Figure 8. Superimposed in red are the negative second derivative and Marr's bound on the second derivative for deflections in inches,

$$D2_{max,in} = 12 \cdot 11 \cdot \frac{\sigma_y}{H \cdot E} = 132 \cdot \frac{36}{66 \cdot 29000} \cong 0.0025 \qquad (20)$$
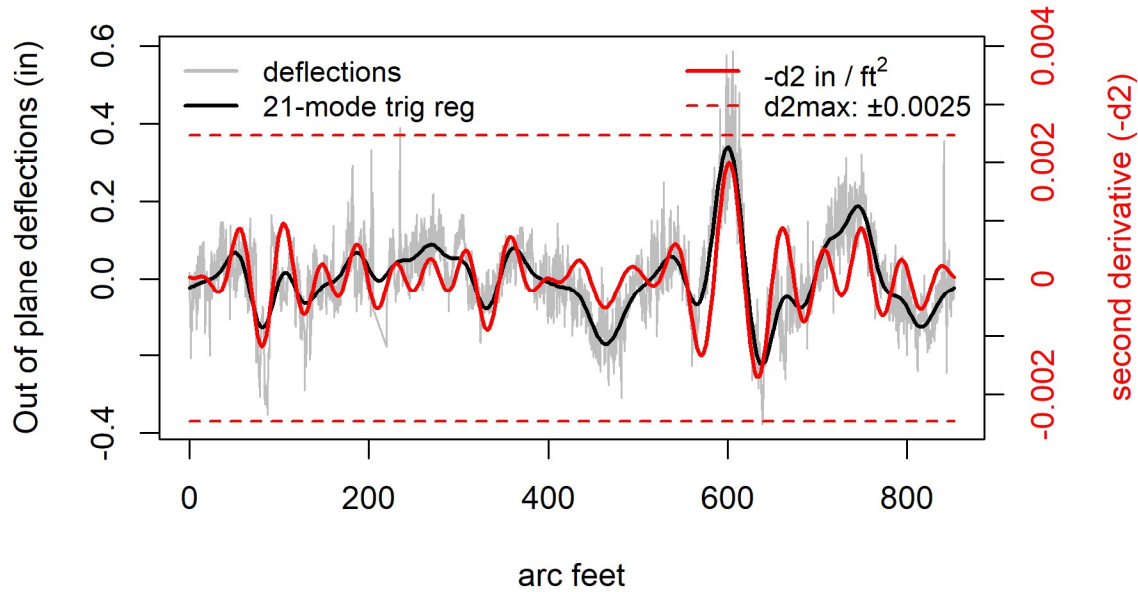

Figure 10. Marr's Criterion with Estimated Second Derivative.

Figure 11 displays second derivatives and second divided differences[17] in a region around the maximum out-of-plane deflection in Figure 10. The graph shows the second derivative $d2 = \hat{u}''(\ell)$ and second divided difference $\Delta 2 = \Delta^2(u)/\Delta \ell^2$ at 8 to 32 feet between stations (L). Clearly, the second difference severely underestimates the second derivative for wider spacing. For example, at 32 ft spacing the second divided difference is less than ½ of the second derivative.

---

[17] See the sentence after Equation (11) for a definition of second divided difference.
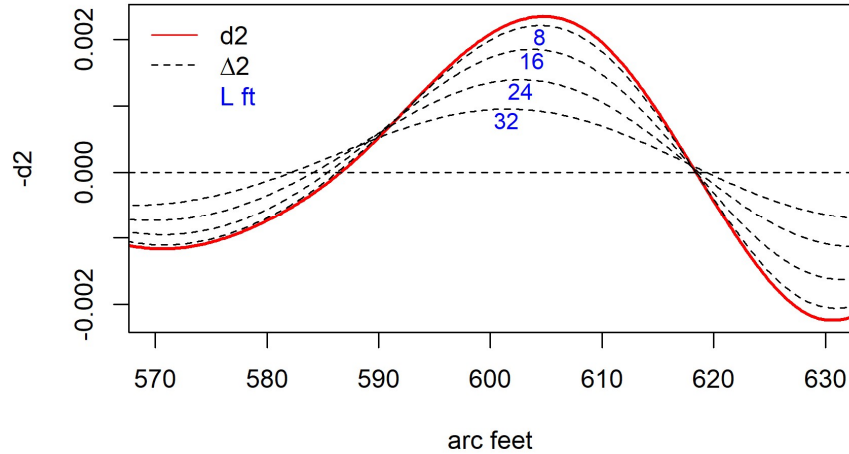
Figure 11. Second difference underestimates second derivative.

More accurate estimation of second derivatives via trigonometric smoothing.

We suggest estimating second derivatives by statistically fitting a finite Fourier series like Equation (17) to the observed deflections from the rigid tilt plane. Cosine terms are included only if they increase the model's overall adjusted R^2 using a method called forward stepwise regression. We analytically calculate the second derivative of the fitted Fourier series to determine the curvature. We call this the *Trigonometric Regression Method.* In light of our analysis of estimation bias[18] and noise sensitivity, we think that, for laser-scan data, this method is less sensitive to arc length than Marr's original method.

$$\hat{u}''(\ell) = -\sum_{k \geq 2}\left(\frac{k}{R}\right)^2 \cdot \hat{A}_k \cdot \cos\left(k \cdot \frac{\ell}{R} - \hat{\varphi}_k\right) \tag{21}$$

Applying Equation (15), we get *Marr's Criterion with Estimated* Derivative for deflections measured in feet,

$$|\hat{u}''(\ell_i)| \leq 11 \cdot \frac{\sigma_y}{H \cdot E} = d2_{\max, ft}, \tag{22}$$

or for deflections measured in inches,

$$|\hat{u}''(\ell_i)| \leq 12 \cdot 11 \cdot \frac{\sigma_y}{H \cdot E} = d2_{\max, in} \tag{23}$$

---

[18] Second derivatives of the trigonometric curve are unbiased estimates of its curvature, but the estimated curve itself could be smoother than the true deflection curve.

PEMY Consulting has developed an R application that calculates the criteria discussed in this chapter. Figure 12 shows the trigonometric regression method applied to the data underlying Figure 8.

The advantage of this method is that it is unnecessary to thin the data to arcs of length L.

Figure 12. Marr's Criterion with Estimated Second Derivative.

The trigonometric regression method is compliant with API 653, paragraph B.2.2.4, because Marr et al. explicitly derived their criterion from the equivalent of our Eq. (22).

When closely spaced observations are available, trigonometric regression should be used instead of three-point curvature estimates with thinning. The trig-reg estimate of curvature is unbiased and less susceptible to noise. In addition, it is more precise because it uses all of the observations, not just three points.

For the data in Figure 12, there is general agreement between Marr (Figure 8), Marr with estimated second derivative (Figure 11), and Andreani (Figure 13) that the maximum deflection near arc length 600 ft. is excessive or nearly so.

In the next section, we demonstrate that Andreani's method is more reliable than Marr's method when the separation between stations is wider than about 20 feet.
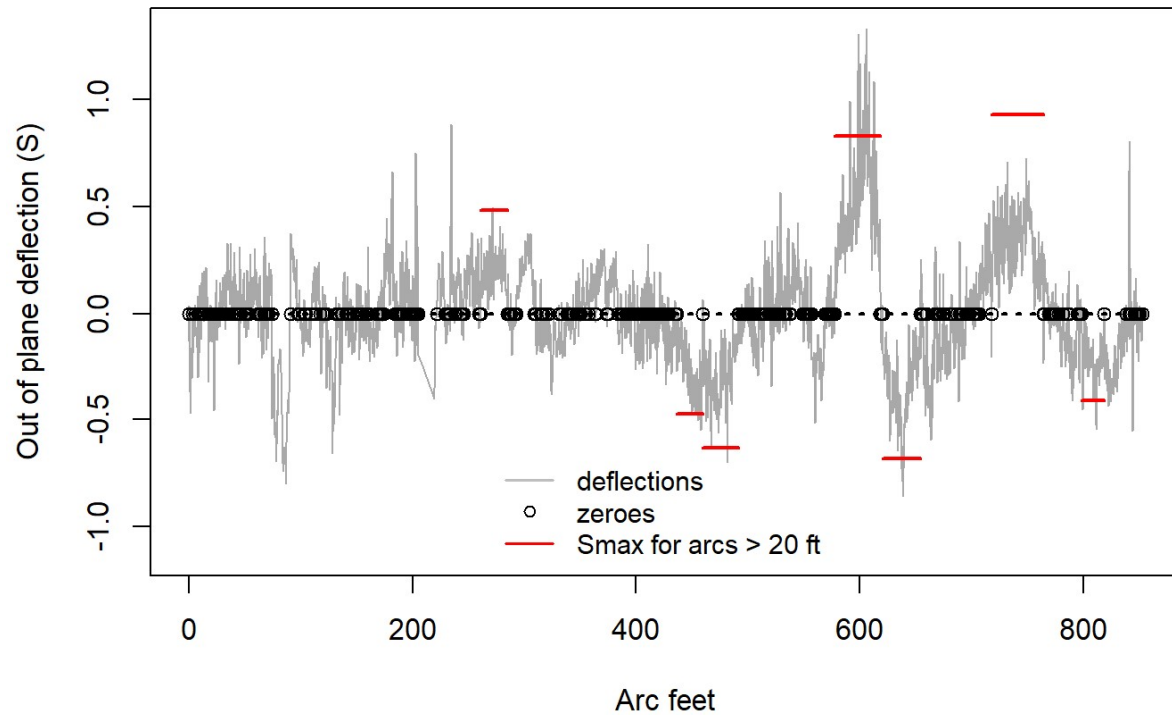

Figure 13. Andreani analysis of laser-scan data.

Comparison of Marr and Andreani Criteria

Referring to Figure 5 and Equation (5), let's define a few symbols,

$$
\begin{aligned}
\ell_{i,left}, \ell_{i,right} &= \text{ left and right endpoints of the i}^{th} \text{ arc} \\
\ell_{i,max} &= \text{ location of max deflection in the i}^{th} \text{ arc} \\
S &= \text{ value of max deflection in i}^{th} \text{ arc (in inches)} \\
U_{i,left}, U_{i,right} &= 0 \ (\text{by definition}) \\
L_{right} &= \ell_{i,right} - \ell_{i,max} \\
L_{left} &= \ell_{i,max} - \ell_{i,left} \\
L &= \left(L_{left} + L_{right} \right)/2 \\
\tilde{L} &= \sqrt{\left(L_{left}^2 + L_{right}^2 \right)/2} \\
S_{arc,ft} &= \ell_{i,right} - \ell_{i,left} \\
S_{max,in} &= K \cdot S_{arc,ft} \frac{D}{H} \frac{\sigma_y}{E}
\end{aligned}
\tag{24}
$$

Now we can interpret Andreani's S, defined in Equation (5), as a second difference of observed out-of-plane settlement values U,

$$
\begin{aligned}
-2 \cdot S &= U_{left} + U_{right} - 2 \cdot U_{max} \\
&= u\left(\ell_{max} + L_{right} \right) - 2u\left(\ell_{max} \right) + u\left(\ell_{max} - L_{left} \right) + noise
\end{aligned}
\tag{25}
$$

Applying the Taylor expansion we get,

$$
\begin{aligned}
-2 \cdot S &= u\left(\ell_{max} + L_{right} \right) - 2u\left(\ell_{max} \right) + u\left(\ell_{max} - L_{left} \right) + noise \\
&\approx \left(L_{right} - L_{left} \right) u'\left(\ell_{max} \right) + \frac{\left(L_{right}^2 + L_{left}^2 \right)}{2} u''\left(\ell_{max} \right) \\
&= \tilde{L}^2 \cdot u''\left(\ell_{max} \right),
\end{aligned}
\tag{26}
$$

since the first derivative $u'\left(\ell_{max} \right)$ vanishes at the maximum.

Average separation between the three points is $L = \left(L_{left} + L_{right} \right)/2$ and,

$$
\frac{L^2}{\tilde{L}^2} = \frac{\left(1 + \rho \right)^2}{2 \cdot \left(1 + \rho^2 \right)}
\tag{27}
$$

where,

$$\rho = \frac{\min\left(L_{left}, L_{right}\right)}{\max\left(L_{left}, L_{right}\right)}$$

(28)

For even spacing; i.e., $L_{left} = L_{right}$, we have $L = \tilde{L}$ and $\rho = 1$.

Finally, by combining equations (5) and (26), Andreani's criterion (in inches) is, approximately,

$$
\begin{aligned}
\left|u''\left(\ell_{max}\right)\right| &\cong \left|\frac{2 \cdot S}{\tilde{L}^2}\right| \\
&\leq \frac{2}{\tilde{L}^2} S_{max,in} \\
&= \frac{2}{\tilde{L}^2} \cdot S_{arc.ft} \cdot K \cdot \frac{D}{H} \cdot \frac{\sigma_y}{E} \\
&= 4 \cdot \frac{L^2}{\tilde{L}^2} \cdot \frac{D}{L} K \cdot \frac{\sigma_y}{H \cdot E} \\
&= \left[4 \cdot \frac{(1+\rho)^2}{2 \cdot (1+\rho^2)} \cdot \frac{D}{L} K\right] \cdot \frac{\sigma_y}{H \cdot E}
\end{aligned}
$$

(29)

where K is number from Table 1. API 653 K table from API 653, Section B.3.2.2.

Marr's criterion for estimated second derivative (in inches) is

$$\left|u''\left(\ell_i\right)\right| \leq 12 \cdot 11 \cdot \frac{\sigma_y}{H \cdot E}$$

(22)

In other words, Andreani, in effect, replaced Marr's constant multiplier, 12·11, with a value that depends on diameter, average distance between the three measurement stations used to calculate S, and the ratio of distances to the left and right endpoint of the arc.

Thus, Andreani's alternative to Marr's multiplier is,

$$Andreani's\ implied\ multiplier = 2 \cdot \frac{(1+\rho)^2}{(1+\rho^2)} \cdot \frac{K \cdot D}{L}$$

(30)

Table 2 lists Andreani's implied multiplier for diameters between 150 and 250 feet, and 16-to-32-foot average separation between the three measurement stations used to compute Marr's deflection measure.

Marr's multiplier for deflections measured in inches is comparable to Andreani's (± 10%) when measurement stations are equally spaced (rho=1) and 20 feet apart. For greater separations Marr's multiplier is too lenient (too big) and therefore Andreani's is the preferred method.

In summary, Marr's method is too lenient when measurement stations are more than 20 feet apart. It will therefore have a higher rate of false negatives (failures to flag excess strain).

				rho				% Difference		
				1	0.75	0.5				
D	K*	Sarc.ft	L	Andreani implied multiplier			Marr			
150	4	32	16	150	147	135	132	-13	-11	-2
150	4	40	20	120	118	108	132	10	11	20
150	4	48	24	100	98	90	132	28	30	38
150	4	56	28	86	84	77	132	42	44	53
150	4	64	32	75	74	68	132	55	56	64
200	3.6	32	16	180	176	162	132	-31	-29	-20
200	3.6	40	20	144	141	130	132	-9	-7	2
200	3.6	48	24	120	118	108	132	10	11	20
200	3.6	56	28	103	101	93	132	25	27	35
200	3.6	64	32	90	88	81	132	38	40	48
250	2.4	32	16	150	147	135	132	-13	-11	-2
250	2.4	40	20	120	118	108	132	10	11	20
250	2.4	48	24	100	98	90	132	28	30	38
250	2.4	56	28	86	84	77	132	42	44	53
250	2.4	64	32	75	74	68	132	55	56	64

Table 2. Andreani's Curvature Bound is Tighter than Marr's.

Andreani's Alternate Method

Andreani et al. thought that the settlement data in Figure 14 did not have a "reliable" tilt plane because $R^2 = 0.617$ is less than 0.90 (see Figure 4). They appear to suggest that the analyst should visually identify *settlement arcs* instead, as in Figure 14. There is no conceptual definition of the term "settlement arc" but API 653 section B.2.2.5.1 does give these instructions,

> a) The actual settlement [not deflections from a tilt plane] *is plotted using points around the tank circumference as the abscissa.*

> b) An initial settlement arc length and maximum settlement is determined from the points on the plotted data that indicate a change in direction of set-tlement slope [see Figure 14].

[Judging from Figure 14, "change in direction" appears to mean a settlement arc is defined by places where the slope changes sign, in other words, at local maxima and minima. For example, S_{arc5} is bounded by local maxima at stations 2 and 10, and has a local minimum at station 6. The arc with greatest absolute deflection is, for unknown reasons, not marked in API 653 Figure B4: it is the dotted red line in Figure 14 that runs from station 5 to station 11 with maximum deflection at station 9.]

c) Additional settlement measurement points may be needed halfway between the points indicating a change in direction of the settlement slope to further refine the settlement arc length and location and magnitude of maximum settlement.

d) Step c) may need to be repeated. The best estimate of the settlement arc length and maximum settlement shall be considered in the procedure given in B.3.2.2 (see Equation (5))

Figure 15 is our rendition of Andreani's standard analysis of deflections from the tilt-plane. Arcs identified by the standard analysis (API 653 Section B.2.2.5) are shown as horizontal black arrows and alternate arcs identified by steps a) – d) are shown as red lines. The alternate analysis missed both positive-going arcs (1 and 3).
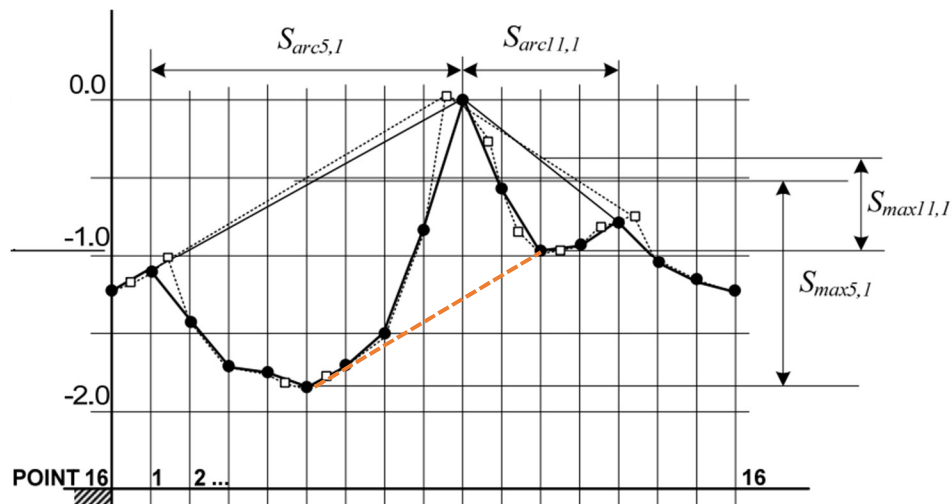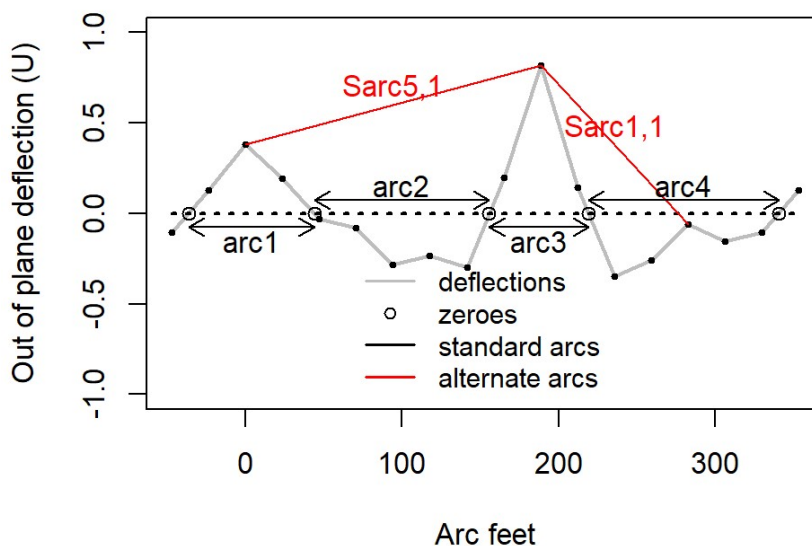

Figure 14. API 653 Figure B.4.

Figure 15. Andreani Standard and Alternate Arcs.

Andreani's standard method based on deflections from the best fitting tilt plane is better calibrated than Marr's method, which is subject to increasing bias as the arc length $(2 \cdot L)$ increases.

Andreani's alternate method, based on identifying local maxima and minima, is demonstrably subjective (see the missed arc in Figure 14) and would be even more so for laser-scan data like Figure 13. In any case it is never necessary because it should always be permissible to work with deflections from a fitted tilt plane.

Andreani's standard method is better calibrated than Marr's. Do not use Andreani's alternate method: always use deflections (U) with the tilt plane removed.

Comments on Differential Settlement.

We have discussed the two differential settlement analyses sanctioned by API 653 Appendix B. The first, Marr's method, is based on Euler-Bernoulli beam theory and a divided second difference estimate of the second derivative or curvature. We have shown that the second difference estimate can be badly biased if the distance between stations, L, is longer than 20 feet.

We conclude that Marr's method is generally unreliable but that it can be made more reliable by replacing Marr's strain estimate (S) with the analytical second derivative of a trigonometric fit (finite Fourier series). For sparce, widely-spaced data we recommend Andreani's method. For dense, closely-spaced data we recommend the *Trig-Fit* Fourier series method in in lieu of using Marr's method.

A second stress analysis method developed by Andreani, et al., is derived from finite-element modelling of simple folds across the tank bottom. It was calibrated to a limiting strain of 3%, based on the API 579 fitness for service criterion and is therefore one step closer to the gold

standard. Andreani's finite element analysis looked only at single folds at different arc lengths but is based on a more realistic model than Marr's method. Unlike Marr's method, it is accurate over a wide range of arc lengths.

API 653 section B.2.2.5 gives this advice:

> *If … the maximum out-of-plane settlement determined in accordance with B.3.2.1 (Marr's method) is exceeded, the procedures given in this section (Andreani's method) may be used in lieu of more rigorous analysis or repair*

We have demonstrated that this advice has it backward: Marr's method is generally too lenient and will sometimes miss overstressed areas that would be identified by Andreani's method. Instead, we recommend that a settlement analysis consist of 1) Andreani's standard analysis, then 2) Marr's analysis, if measurement stations are separated by 16 to 20 feet, and then 3) the Trig-Reg method, when measurements are closely spaced. A tank gets a clean bill of health only if both Andreani's and the Trig-reg analyses do not indicate overstress.

All of these analyses – Marr, Andreani, and Trig-Reg – are screening tests to identify possible excess stress. The gold standard is finite element analysis.

References

[1] W. A. Marr, J. A. Ramos and T. W. Lambe, "Criteria for Settlement of Tanks," *ASCE, Journal of Geotechnical Engineering Division, Proceedings of the American Society of Civil Engineers,,* vol. 108, no. GT8, 1982.

[2] J. Andreani and N. Carr, "Final Report on the Study of Out-of-Plane Tank Settlement," , Report to API SCAST," API SCAST, May, 2007.

[3] Z. Malik, J. Morton and C. Ruiz, "Ovalization of Cylindrical Tanks as a Result of Foundation Settlement," *Journal of Strain Analysis,* vol. 12, no. 4, p. 339–348, 1977.

[4] A. M. D'Orazio and J. M. Duncan, "Discussion (of "Criteria for Settlement of Tanks by Marr, Ramos, & Lambe")," *Journal of the Geotechnical Engineering Division, ASCE,* vol. 108, no. 8, August 1982.

[5] "API Standard 653, 5th Ed., Nov. 2014, Addendum 2, May. 2020".

[6] M. Jonaidi and P. Ansourian, "Harmonic settlement effects on uniform and tapered tank shells," *Thin-Walled Structures,* vol. 31, p. 237–255, 1998.

[7] J. Andreani and N. Carr, "Study of Out-of-Plane Tank Settlement," API, Washington, D.C., May 2007.

Appendix:
Propagation of Error & Operating Characteristics of Marr's Method

Effect of Measurement Error, Roughness, and Spacing on the Marr Method

Using the "signal plus noise" model in Equation (7), observed deflection can be written as true deflection plus noise. Noise consists of measurement error plus intrinsic roughness: welds, dings, patches, etc. Observed deflections U are true deflection plus noise, $U = u(\ell) + e$

$$
\begin{aligned}
S_i &= U_i - (U_{i+1} + U_{i-1})/2 \\
&= \left[u(\ell_i) - (u(\ell_{i+1}) + u(\ell_{i-1}))/2 \right] + \left[e_i - (e_{i+1} + e_{i-1})/2 \right] \qquad (31) \\
&= \left[\text{true deflection} \right] + \left[\text{noise} \right]
\end{aligned}
$$

Assuming that noise is random with standard deviation sd_e, the standard deviation of an out-of-plane deflection is,

$$
sd(S_i) = sd(-0.5 \cdot e_{i+1} + e_i - 0.5 \cdot e_{i-1}) = sd_e \cdot \sqrt{1.5} \qquad (32)
$$

Controlling false positives and false negatives requires that the noise component of S_i be much smaller than the critical value for S, S_{max}

$$
sd_e << \frac{11 \cdot \sigma_y}{E \cdot \sqrt{1.5}} = \frac{L^2}{H} \cdot 0.0112 \qquad (33)
$$

Operating Characteristic: Probability of a Positive Test for Over-Strain

If noise is Gaussian, the probability of a positive test for over-strain is,

$$
\begin{aligned}
P(S > S_{max}) &= P\left(\frac{S - \mu_S}{sd_S} > \frac{S_{max} - \mu_S}{sd_S} \right) \\
&= P\left(Z > \frac{S_{max}}{sd_S} \cdot \left(1 - \frac{\mu_S}{S_{max}} \right) \right) \qquad (34) \\
&= P(Z > SNR \cdot SM)
\end{aligned}
$$

where, SNR is the Signal to Noise Ratio, and SM is the Safety Margin; i.e., the relative distance of true strain μ_S from maximum permitted strain S_{max}

Table 3 shows the effect of SNR and SM on false positives[19] and false negatives[20].

For example, if true stress is 20% below Smax (SM = 0.2) the false positive rate is 12% for SNR=6 sigma and 27% for SNR=3 sigma, with noisy data (SNR=3) 27% of tests will be false positives and 73% will be true negatives. An acceptable level of false positives depends on a cost-benefit analysis of the protocol for following up an apparent positive. For another example, if true stress is 30% above the limit, Smax, and SNR=3 sigma, there will be 18% false negatives and 82% true positives. An acceptable level of false negatives depends on a cost benefit analysis of protocol for following up an apparent negative.

SM	SNR = 6	SNR=3	
0.5	0	7	% False Positive
0.4	1	12	
0.3	4	18	
0.2	12	27	
0.1	27	38	
0	50	50	
-0.1	27	38	% False Negative
-0.2	12	27	
-0.3	4	18	
-0.4	1	12	
-0.5	0	7	

Table 3. Effect of Signal-to-noise Ratio on False Positive & Negative Rates.

Clearly it is desirable to reduce both false positive and negative rates. That requires reducing noise. Table 3 suggests that a signal to noise ratio at least 6 is needed to avoid excess false positives. then shows the maximum permissible noise standard deviation required to achieve given signal to noise ratios. We shall see that there are strategies for reducing SNR.

Mitigating the Signal to Noise Ratio.

Noise is a combination of intrinsic roughness[21] and measurement error and probably cannot be reduced below 0.25 inch. Table 4 indicates that 5 sigma or better SNR is out of reach for L less

---

[19] A false positive occurs if the true deflection, μ_S is less than S_{max} but observed deflection, S, is above S_{max}

[20] False negatives can happen when the tank is truly over the stress limit (SM <0) but observed stress is less than Smax.

[21] Intrinsic roughness due to overlapping plates etc. is ± 0.25

than 20 feet, and apparently the bigger L is the better. However, this is counterbalanced by increasing bias in the 3-point curvature estimate as L increases, see Figure 11.

It seems, therefore that for methods based on 3-point curvature estimates, the sweet spot between noise and bias is at L = 20 feet. We showed that there is a more sophisticated curvature estimate that gets around this problem if the distance between measurement stations is very small, as with laser-scan data.

L ft	H = 40 ft				H = 50 ft			
	SNR				SNR			
	3	4	5	6	3	4	5	6
16	0.29	0.22	0.17	0.14	0.23	0.17	0.14	0.12
20	0.45	0.34	0.27	0.22	0.36	0.27	0.22	0.18
24	0.65	0.49	0.39	0.32	0.52	0.39	0.31	0.26
28	0.88	0.66	0.53	0.44	0.71	0.53	0.42	0.35
32	1.15	0.86	0.69	0.58	0.92	0.69	0.55	0.46
36	1.46	1.09	0.87	0.73	1.17	0.87	0.70	0.58

Table 4. Maximum Permissible Noise Standard Deviation (inches) for Given SNR, L, and H

Marr et al.'s K value Does Not Adjust for Bias Caused by Large L

Marr, et al., computed lower bounds for factor K using data from 38 floating-roof and more than 60 cone-roof tanks that had not ruptured. The logic was that the stress observed in an intact tank must be less than the failure stress. Rearranging equation (13) implies that for all 38 tanks (t) in the calibration set,

$$K > K_{t,observed} = \frac{S_t}{L_t^2} \cdot \frac{H_t \cdot E}{\sigma_f} \tag{35}$$

Observed K values are listed in Table 5. Marr, et al.'s Calibration Set (adapted from their Figure 6, all dimensions in feet).Table 5 and are plotted against arc length (L) in Figure 16. The red curve is logically a lower bound on K because the 38 tanks had not ruptured but would have ruptured at some higher value of K.
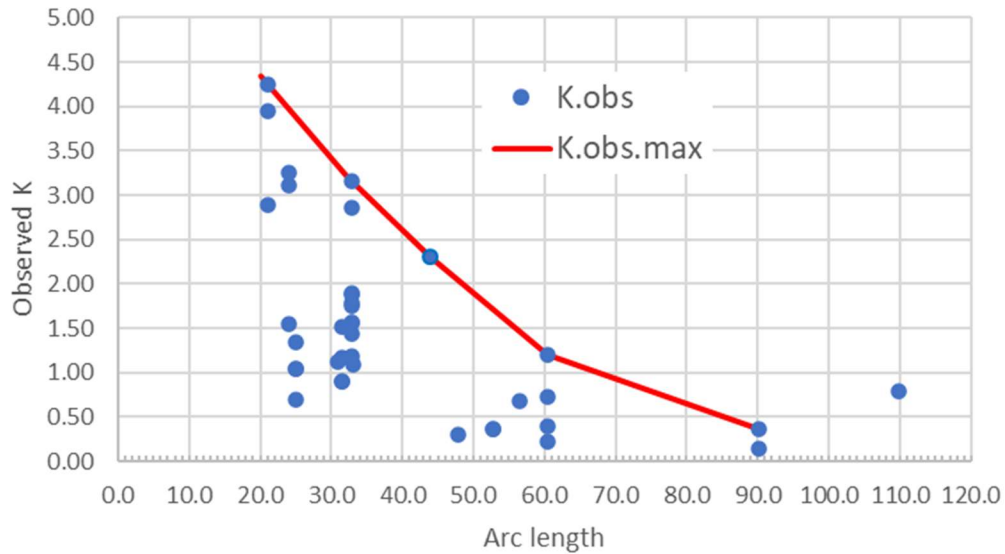
Figure 16. Computed lower bound on K for 38 Floating-Roof tanks.

D'Orazio and Duncan [4], pointed out that K decreases quadratically as arc length increases, as shown in Figure 16. They reasoned that noise standard deviation, sd_e, is leveraged by L^{-2}, making $K_{observed}$ more dispersed for small L-values. That might account for some of the decrease, but we have found that the true explanation is the fact that the second divided difference is a biased estimate of the second derivative (see Figure 11).

In the section titled Adapting Marr's Criterion to Laser-Scan Data, we demonstrate that the pattern in Figure 16 comes from using an approximation for the second derivative and, consequently, factor K should be a function of the distance L between measurement stations.

tank	Diam	Height	L arc	S.obs	K.obs	tank	Diam	Height	L arc	S.obs	K.obs
1	133.5	55.1	21.0	0.0207	4.25	20	209.6	60.0	32.8	0.0191	1.75
2	133.5	55.1	21.0	0.0193	3.95	21	209.6	60.0	32.8	0.0205	1.88
3	133.5	55.1	21.0	0.0141	2.89	22	209.6	60.0	32.8	0.0195	1.79
4	152.6	54.8	24.0	0.0099	1.55	23	209.6	60.0	32.8	0.0170	1.56
5	152.6	54.8	24.0	0.0199	3.12	24	209.6	60.0	32.8	0.0130	1.19
6	152.6	54.8	24.0	0.0208	3.26	25	209.6	60.0	32.8	0.0156	1.43
7	80.1	42.0	25.1	0.0095	1.04	26	169.0	47.9	33.1	0.0151	1.08
8	96.1	42.0	25.1	0.0095	1.04	27	167.3	48.6	44.0	0.0558	2.30
9	80.1	54.1	25.1	0.0095	1.34	28	244.4	47.9	47.9	0.0087	0.30
10	80.1	42.0	25.1	0.0064	0.70	29	67.3	39.4	52.8	0.0159	0.37
11	315.6	72.2	30.8	0.0090	1.13	30	67.3	39.4	52.8	0.0159	0.37
12	219.8	54.1	31.5	0.0130	1.17	31	144.4	54.1	56.4	0.0244	0.68
13	219.8	54.1	31.5	0.0100	0.90	32	229.7	48.6	60.4	0.0180	0.39
14	219.8	54.1	31.5	0.0100	0.90	33	229.7	48.6	60.4	0.0551	1.20

15	180.4	54.1	31.5	0.0170	1.52	34	229.7	48.6	60.4	0.0330	0.72
16	209.6	60.0	32.8	0.0170	1.56	35	229.7	48.6	60.4	0.0100	0.22
17	209.6	60.0	32.8	0.0207	1.89	36	229.7	48.6	90.2	0.0140	0.14
18	209.6	60.0	32.8	0.0313	2.86	37	229.7	45.9	90.2	0.0400	0.37
19	209.6	60.0	32.8	0.0345	3.16	38	139.8	48.2	109.9	0.1218	0.80

Table 5. Marr, et al.'s Calibration Set (adapted from their Figure 6, all dimensions in feet).